Downloaded from www.ajronline.org by 45.27.234.97 on 06/22/18 from IP address 45.27.234.97. Copyright ARRS. For personal use only; all rights reserved

AJR FOCUS ON:

Update on CT and MRI of Adrenal Nodules

Nicola Schieda[1]
Evan S. Siegelman[2]

OBJECTIVE. The objective of this article is to review the current role of CT and MRI for the characterization of adrenal nodules.

CONCLUSION. Unenhanced CT and chemical-shift MRI have high specificity for lipid-rich adenomas. Dual-energy CT provides comparable to slightly lower sensitivity for the diagnosis of lipid-rich adenomas but may improve characterization of lipid-poor adenomas. Nonadenomas containing intracellular lipid pose an imaging challenge; however, nonadenomas that contain lipid may be potentially diagnosed using other imaging features. Multiphase adrenal washout CT can be used to differentiate lipid-poor adenomas from metastases but is limited for the diagnosis of hypervascular malignancies and pheochromocytoma.

Incidental adrenal nodules are detected in approximately 4–5% of patients undergoing CT examinations. The prevalence of adrenal incidentalomas increases with age; fewer than 0.5% of adrenal nodules are discovered in patients in their 20s compared with up to 7% in patients older than 70 years old [1–4]. Although benign adenomas are overwhelmingly the most common adrenal nodule encountered in the general population [3, 5, 6], the possibility of other pathologic entities (including pheochromocytoma, adrenocortical carcinoma [ACC], and metastatic disease) requires that radiologists develop an approach to the characterization of adrenal lesions. Having an understanding of the various techniques used to image adrenal nodules with CT and MRI, the inherent strengths and limitations of these techniques, key distinguishing imaging features, and emerging techniques that may be used for improved adrenal nodule characterization is important. The purpose of this article is to present conventional and evolving technical aspects of adrenal imaging at both CT and MRI, discuss the role of CT and MRI for the diagnosis of common adrenal pathologic entities, and review the most current literature on the topic.

CT

CT characterization of adrenal nodules can be performed without or with the use of iodinated contrast material. Unenhanced CT characterization of adrenal nodules relies on the detection of intracytoplasmic lipid found within adrenal adenomas, which reduces their CT attenuation. In lipid-rich adenomas, attenuation measurements will be less than 10 HU. This quantitative threshold is highly specific for the diagnosis of adenoma [7]. Attenuation measurements are performed by ROI analysis. ROIs should be placed within the nodule encompassing two-thirds of its circumference to obtain a measurement that is as accurate and representative as possible [8].

In approximately one-third of adenomas, there is insufficient intracytoplasmic lipid content so that CT attenuation values will be greater than 10 HU (i.e., lipid-poor adenomas) [7, 8]. A proportion of these adenomas can be further characterized using MRI, which we discuss later, because chemical-shift imaging (CSI) has been shown to be more sensitive for the detection of intracytoplasmic lipid than unenhanced CT [9]. Lipid-poor adenomas can also be characterized using a dedicated adrenal washout CT protocol [6, 10] that has been shown to be better for the characterization of adenomas measuring greater than 20 HU compared with CSI [11]. At multiphase adrenal washout CT, adenomas show washout of contrast material over time; multiphase adrenal washout CT has been previously validated as a specific method to differentiate lipid-poor adenomas from metastatic disease using quantitative absolute and relative washout criteria [6, 10, 12,

Keywords: adenoma, adrenal, CT, dual-energy CT, MRI

DOI:10.2214/AJR.16.17758

Received December 3, 2016; accepted without revision December 19, 2016.

[1]Department of Radiology, The Ottawa Hospital, The University of Ottawa, 1053 Carling Ave, Civic Campus C1, Ottawa, ON K1Y 4E9, Canada. Address correspondence to N. Schieda (nschieda@toh.on.ca).

[2]Department of Radiology, Hospital of the University of Pennsylvania, University of Pennsylvania, Philadelphia, PA.

AJR 2017; 208:1206–1217

0361–803X/17/2086–1206

© American Roentgen Ray Society

Downloaded from www.ajronline.org by 45.27.234.97 on 06/22/18 from IP address 45.27.234.97. Copyright ARRS. For personal use only; all rights reserved

13] (Fig. 1). The CT washout technique can be performed using unenhanced CT (to establish benign absolute washout of > 60%) or using only 70-second and 15-minute contrast-enhanced CT (CECT) (to calculate relative washout of > 40%) [6, 10]; however, CECT should not be performed using earlier delays (e.g., < 15 minutes) because earlier delays reduce accuracy [14]. The application of CT washout to other clinical situations (e.g., to diagnose pheochromocytoma or ACC or to differentiate lipid-poor adenomas from hypervascular metastases) can be problematic, which is discussed later.

The use of CT histogram analysis of attenuation values for adrenal nodules that measure more than 10 HU at unenhanced CT has been previously studied [15]. Histogram analysis of attenuation values (rather than of the mean attenuation values) should theoretically detect smaller amounts of intracytoplasmic lipid within a lipid-poor adenoma. Previous studies have shown that CT histogram analysis of a nodule showing more than 10% negative pixel count is specific for adenoma; however, low sensitivity for diagnosis has limited the application of this method in routine clinical practice [16, 17].

A common dilemma encountered in clinical practice occurs when an adrenal nodule is detected at single-phase CECT because the attenuation value of an adenoma at CECT rarely measures less than 10 HU (Fig. 2). In these instances, a patient may need to be recalled to undergo dedicated unenhanced CT or CSI to confirm the diagnosis of adenoma [5]. As the application of dual-energy CT (DECT) becomes more widespread in clinical practice, this scenario may be resolved through the use of a variety of previously described techniques [18]. The most common and practical method for diagnosing adenoma at DECT is by attenuation measurements on virtual unenhanced CT (Fig. 2). Until recently, virtual unenhanced CT was available only using the dual-source platform but is now available using several vendors' technology. Multiple studies have shown comparable, albeit slightly lower, sensitivity (with no false-positive interpretations) for the diagnosis of adenoma when measuring attenuation values on dual-source virtual unenhanced CT compared with true unenhanced CT [19–23]. In a recent meta-analysis that we performed, the slightly lower sensitivity of virtual unenhanced CT was shown to possibly relate to higher attenuation values on virtual unenhanced CT derived from earlier phases of enhancement [24]. Using single-source fast-kilovoltage-switching DECT, Glazer et al. [25] reported that adenomas differed significantly from nonadenomas on virtual monochromatic spectral imaging performed at 140 keV and using iodine-subtracted datasets (derived from a iodine-water basis pairing). In their study, there was no difference in the ability to discriminate adenomas from nonadenomas when compared by the timing of contrast-enhanced imaging. The authors suggest that differences related to the timing of contrast injection at dual-source DECT may differ by the method of material decomposition algorithms used by each vendor; however, they acknowledge that their study was underpowered to show this effect [25].

More recently, the use of lipid concentration measurements (in milligrams per milliliter) has also been described as a viable method to differentiate lipid-rich adenomas from nonadenomas [26]. In a study by Mileto et al. [27], both lipid-rich and lipid-poor adenomas could be differentiated from nonadenomas using material density analysis of fat-water basis pairs, and this analysis outperformed unenhanced CT. These advanced techniques show promising preliminary results but require further evaluation and study on different vendor platforms if they are to become used routinely in clinical practice.

MRI

The most important MRI technique used to characterize adrenal lesions is CSI. In 1992, Mitchell and colleagues [28] showed that CSI could detect intracellular lipid that is present in most adrenal adenomas and differentiate them from metastatic disease and pheochromocytoma, which do not typically contain lipid. CSI of the adrenal glands should be performed as a dual-echo gradient-recalled echo sequence in which both echoes are obtained in the same breath-hold. This protocol ensures adequate coregistration of data on in-phase and opposed-phase images and enables the derivation of subtraction (in-phase minus opposed-phase) lipid-only images [29]. The opposed-phase TE should be shorter than the corresponding in-phase TE to ensure that the loss of signal intensity on the opposed-phase image is from lipid-water cancellation and not from T2*-induced susceptibility effects [30–32]. At 1.5 T, this is readily achieved using 2D or volume-interpolated 3D sequences with TEs of approximately 2.2 and 4.4 ms.

In an older study by Ramalho et al. [33], 2D CSI outperformed 3D CSI in terms of overall image quality and the number and severity of artifacts; however, in our experience with current-generation scanners, 2D and 3D CSI techniques provide comparable image quality but using 3D interpolated sequences provides the advantages of higher resolution and higher signal-to-noise ratio, which can potentially result in improved characterization of small lesions. Current-generation 3-T systems should also be able to obtain the first opposed-phase and in-phase TE pair (at ≈ 1.1 and 2.2 ms [34]); however, on older 3-T systems, previously described modifications to the base pulse sequence may be required to achieve correct sampling of the first opposed-phase–in-phase echo pair [32].

The use of 3-point Dixon techniques for CSI of the adrenal glands has been described by Namimoto et al. [35] who reported accuracy comparable to that of 2D CSI for the diagnosis of adenoma. It is debatable what additional value 3-point Dixon techniques will offer compared with conventional dual-echo CSI in clinical practice because adrenal adenomas would not be expected to show a combination of both iron deposition and intracellular lipid, the findings that make 3-point techniques particularly valuable.

To establish the presence of intracellular lipid on CSI, one can visually inspect or measure the change in signal intensity of the lesion from the in-phase image to the opposed-phase image (by the signal-intensity index or adrenal-to-spleen signal-intensity ratio). A signal-intensity index of greater than 16.5% and adrenal-to-spleen signal-intensity ratio of less than 0.71 are previously described thresholds at 1.5 T that optimize diagnosis of adenoma [36]. Investigators have reported that the chemical-shift index threshold level at 3 T for differentiating adenomas from nonadenomas is lower than 16.5% and that applying a 16.5% threshold at 3 T may fail to classify a proportion of lipid-containing adenomas [34]. Alternatively, one can use subtraction imaging to facilitate the detection of intracellular lipid [31, 37].

When comparing subjective and quantitative analyses, we agree with Mayo-Smith et al. [38] that often qualitative evaluation gives a similar result to quantitative results. As an alternative to washout CT for the evaluation of an adrenal lesion that measures 10 HU or more at unenhanced CT, CSI can be performed because it has been previously shown to differentiate adenomas from nonadeno-

Downloaded from www.ajronline.org by 45.27.234.97 on 06/22/18 from IP address 45.27.234.97. Copyright ARRS. For personal use only; all rights reserved

mas with good sensitivity, particularly for lesions that measure between 10 and 30 HU [9]. CSI is unlikely to detect intracellular lipid within an adrenal mass if the attenuation is 30 HU or greater at unenhanced CT [39] and was more recently shown to be less effective than washout CT for adenomas measuring more than 20 HU [11].

We have encountered a seemingly paradoxical observation when the adrenal glands show signal-intensity loss on the longer-TE in-phase images compared to the shorter-TE opposed-phase images [40, 41]. This finding can occur in patients who have been administered ferumoxytol, which is an ultrasmall iron oxide particle parenteral agent that is used to treat chronic anemia [42] (Fig. 3). More recently, Perillo et al. [43] presented their observations that the adrenal glands may also show susceptibility effects due to iron deposition in hemosiderosis and that this finding in their series always occurred in the presence of iron deposition in other organs.

The yield of MRI techniques other than CSI for the characterization of adrenal masses is controversial. At T2-weighted MRI, adrenal adenomas tend to be homogeneous and to show intermediate to low signal intensity compared with skeletal muscle or liver [44, 45]; however, when large, adenomas may undergo cystic degeneration and appear heterogeneous [46]. The use of DWI to differentiate adenomas from nonadenomas has not been successful because significant overlap in quantitative apparent diffusion coefficient (ADC) values has been reported [47, 48]. Although Sandrasegaran et al. [48] showed that for adrenal lesions with indeterminate findings at CSI, higher ADC values were observed in adenomas, this finding has not to our knowledge been reproduced. Preliminary studies have shown some success when using dynamic gadolinium-enhanced MRI for differentiating adenomas from metastases [49, 50]; however, both of these studies combined quantitative enhancement evaluation with subjective imaging features, which necessitates that these observations be validated by other groups.

Adrenocortical Adenoma

The majority of incidentally discovered adrenal lesions are benign adrenal adenomas [51]. The typical imaging features of adenoma have been described in the previous CT and MRI sections and include the following: small size (usually < 4 cm), homogeneous and well-circumscribed, presence of intracellular lipid, low to intermediate signal intensity on T2-weighted images, and washout of contrast material on CT studies performed using a dedicated multiphase adrenal CT protocol. Avid enhancement of adrenal adenomas on early (60–75 seconds) contrast-enhanced imaging is not rare; therefore, the degree of early enhancement in adenomas can overlap with other hypervascular adrenal lesions such as pheochromocytoma [52–55] (Fig. 1). Adrenal adenomas can be functioning or nonfunctioning; one insensitive but specific imaging finding that indicates an adrenal lesion may be hyperfunctioning is the presence of hypoplasia of the remainder of the adrenal gland parenchyma [29, 56].

Less commonly, adrenocortical adenomas may show atypical features. A heterogeneous appearance of adenomas (i.e., mixed areas of low [< 10 HU] and higher [≥ 10 HU] attenuation or heterogeneous signal-intensity drop on opposed-phase CSI) can be observed (Fig. 4). When an adrenal lesion shows mixed attenuation or heterogeneous signal-intensity drop on CSI, the possibility of an adrenal collision tumor, which we discuss later, should be considered; however, in a study by Gabriel et al. [57] heterogeneous signal-intensity drop was observed in 14% of adrenal nodules and was most commonly associated with a benign diagnosis. Calcification in adrenal adenomas has been previously described and is considered rare but may be usually present in large adenomas that have undergone degeneration [46]. In a large retrospective series of 106 calcified adrenal masses, among adult patients, adenomas were the second most commonly calcified adrenal masses after adrenal cysts [58]; however, calcification can occur in other adrenal nodules including myelolipoma, ACC, and metastases [59]. Large size and the presence of internal cystic change or necrosis are additional atypical features of adenomas [46]. In a retrospective study from the archives of the Armed Forces Institute of Pathology, large adenomas showing calcification, heterogeneity, and internal cystic change or necrosis could not be differentiated from ACC at CT or MRI, and resection was suggested for these lesions [46].

Myelolipoma

Adrenal myelolipoma is a relatively uncommon benign adrenal neoplasm composed of fat and hematopoietic tissue [60]. Patients are generally asymptomatic unless they develop pain from intratumoral hemorrhage or have symptoms due to mass effect when lesions are larger than 10 cm. Diagnosis of myelolipoma is established by showing fat attenuation (< –10 to –20 HU) at CT or macroscopic fat at CSI and fat-suppression MRI [61]. The diagnosis of myelolipoma can be confidently made when an adrenal mass is composed of at least 50% fat (Fig. 5). In a CT series of 64 adrenal myelolipomas, 25% (16/24) of lesions with less than 10% fat were actually cases of myelolipomatous metaplasia in the setting of other adrenal neoplasms [58] (Fig. 6), which can include both adenomas and ACC [62, 63]. The presence of bulk fat in ACC, which we discuss later, has been previously described in three case reports [64–66].

Pheochromocytoma

Pheochromocytomas can be challenging to diagnose prospectively at CT or MRI [67, 68]. Symptomatic pheochromocytomas are confirmed using biochemical testing including 24-hour urine fractionated metanephrine or catecholamine values, which have sensitivity and specificity rates of more than 90% [69]. Incidental pheochromocytomas can be encountered on imaging studies [70, 71] and despite variable appearance do show some features that may suggest the diagnosis. At multiphase CT, pheochromocytomas are hyperenhancing and show washout of contrast material; however, there is substantial overlap with adrenal adenomas. For example, approximately one-third of pheochromocytomas will show washout in the adenoma range, and adenomas can enhance avidly on the 70-second phase of enhancement [52–55]. Therefore, pheochromocytomas cannot be reliably differentiated from adenomas using CT washout protocols [52–55] (Fig. 7). The presence of intracytoplasmic lipid effectively excludes the diagnosis of pheochromocytoma [55] because this finding has been described in only two previous case reports [72, 73]. Pheochromocytomas show increased signal intensity, which has been referred to as being "light-bulb bright" [44], on T2-weighted images; however, approximately one-third of pheochromocytomas do not have this appearance [44]. Moreover, large adenomas may also show increased signal intensity at T2-weighted imaging because of cystic changes [46]. More recently, in a study by Borhani and Hosseinzadeh [74] and in our own study [55] that the use of a quantitative T2-weighted signal-intensity ratio could be useful to differentiate pheochromocytoma from adenoma. Scintigraphic studies using ^{123}I-metaiodobenzylguanidine (MIBG)

Downloaded from www.ajronline.org by 45.27.234.97 on 06/22/18 from IP address 45.27.234.97. Copyright ARRS. For personal use only; all rights reserved

are often performed to confirm the diagnosis because of accuracy rates of more than 95% [75]; however, CT and MRI may be beneficial in selected patients with coexisting adenomas and for surgical planning.

Metastases

The adrenal glands are a common site for metastatic disease. The first presentation of an unknown malignancy as an incidental adrenal metastasis is exceedingly rare and would be worthy of a case report. Song et al. [51] evaluated more than 1000 consecutive patients with an incidental adrenal nodule detected at imaging who had no personal history of malignancy and found that not a single malignant lesion was detected. Moreover, in a large retrospective series from MD Anderson Cancer Center of patients presenting with an occult malignancy, the adrenal gland was involved in only 6% (95/1639) of patients [76]. Furthermore, in that study involvement was limited to the adrenal glands in only 0.2% (4/1639), and in these patients 100% of masses were 6 cm or larger and 75% of masses were bilateral [76].

When a personal history of malignancy is present, differentiation of adrenal adenoma from metastatic disease can typically be achieved using CT or MRI. A nodule measuring less than 10 HU at unenhanced CT can be diagnosed as a lipid-rich adenoma with high specificity [7]. With CSI, the presence of intracellular lipid is also highly specific for adrenal adenoma; however, this finding is limited when metastases from primary malignancies contain intracellular lipid or fat (e.g., clear cell renal cell carcinoma [RCC] [77] and hepatocellular carcinoma [HCC] [78, 79]). We recently described the use of other MRI features—including increased T2 signal intensity and heterogeneity—to differentiate clear cell RCC metastases from adenomas despite the fact that both nodules may contain intracellular lipid [80] (Fig. 8). A well-known limitation of washout CT occurs in hypervascular metastases, such as clear cell RCC and HCC [81], because hypervascular metastases are also expected to show washout of contrast material that may cross over into the adenoma range. Other features associated with adrenal metastases from RCC at multiphase CT included larger size, irregular margins, invasive features, and heterogeneous internal texture [82].

An adrenal collision tumor is defined as two adjacent adrenal tumors that are histologically distinct [32]. The most common adrenal collision tumor occurs when there is a metastasis identified in an adrenal gland containing an adrenal adenoma. In a series of 104 patients with adrenal adenoma and primary malignancy, Schwartz et al. [83] showed an incidence of collision tumors of approximately 2%. Collision tumors are rare in clinical practice but may be suspected in cases in which an adrenal nodule shows heterogeneous low density or heterogeneous signal-intensity drop at CSI in a patient with a history of malignancy (Fig. 9). The diagnosis of collision tumor may be established by histologic confirmation with selective biopsy of the soft-tissue portion of the lesion, surgery, or follow-up imaging.

Adrenocortical Carcinoma

ACC is a rare aggressive malignancy with an annual incidence of 1 case per 1 million individuals [84]. ACCs are commonly sporadic but can be associated with multiple endocrine neoplasia type 1, Lynch syndrome, and Li-Fraumeni syndrome [85]. ACCs are treated with surgical resection, and surgical resection can be potentially curative in patients with localized disease [86]. The CT and MRI features of ACC have been previously reviewed in this journal [87]. Independent of imaging modality, ACCs are usually large. At unenhanced CT, ACCs have attenuation levels greater than 10 HU and have slower relative and absolute washout rates than adenomas at adrenal washout CT [4, 88]. At CSI, some ACCs may show intracellular lipid and hemorrhage [61, 89] (Fig. 10). The presence of macroscopic fat in ACC is rare and has been documented only in case reports [64–66].

In a recent institutional review of 439 ACCs from MD Anderson Cancer Center, 5.7% (25/439) of patients with ACCs underwent imaging before diagnosis that showed either normal adrenal glands (20% [5/25]) or a nodule that was smaller than 4 cm (56% [14/25]) [90]; however, none of the adrenal nodules that were less than 4 cm and were precursors to ACC in this series showed intracellular lipid at unenhanced CT. For benign-appearing indeterminate adrenal masses measuring less than 4 cm (e.g., homogeneous, smooth margins) at cross-sectional imaging, the American College of Radiology (ACR) White Paper suggests follow-up CT or MRI in 12 months and states that stability in size and appearance over a period of 12 months or longer is a reassuring feature of benignity [5]. This strategy is concordant with recently published clinical practice guidelines in which a 6- to 12-month follow-up study is suggested to assess for growth in indeterminate non–lipid-containing adrenal nodules for which adrenalectomy is not performed [91]. That same expert panel acknowledged a lack of evidence regarding size or volume thresholds at follow-up imaging but suggested that an increase of more than 20% in the diameter together with an at least 5-mm increase in this diameter were suspicious features [91]. For lesions measuring larger than 4 cm, the ACR White Paper suggests consultation for potential surgical resection unless a diagnosis of metastatic disease can be established [5]. It is acknowledged that the widely cited 4-cm cutoff that signifies an increased risk of malignancy is not based on good clinical evidence [91]; nevertheless, surgical series have shown this threshold to be sensitive for the diagnosis of adrenal malignancies [92].

Conclusion

CT and MRI of the adrenal glands remain integral for the characterization of adrenal nodules in clinical practice (Table 1). Most incidentally discovered adrenal nodules are benign adenomas. In patients with no personal history of malignancy, a first presentation of cancer of an unknown primary origin as an incidental adrenal metastasis is extremely rare. In patients with malignancy, attenuation of less than 10 HU at unenhanced CT or a signal-intensity drop at CSI is a specific finding of adenoma. A signal-intensity drop at CSI can also be seen in metastases from tumors that contain lipid; however, other features of metastases such as larger size, increased T2 signal intensity, and heterogeneity may enable diagnosis. In lipid-poor adenomas, washout CT can differentiate adenomas from metastases except in cases of hypervascular tumors in which metastases can show washout in the adenoma range. Size, irregular margins, invasive features, and tumor texture may also help to diagnose metastases in this setting. The imaging features of pheochromocytomas overlap with those of adenomas at washout CT, and diagnosis is usually established through a combination of biochemical testing and MIBG scanning. Increased T2 signal intensity and the absence of intracytoplasmic fat are features that suggest pheochromocytoma at CT or MRI. Myelolipomas are diagnosed by detecting a large amount of macroscopic or bulk fat within an adrenal nodule; in larger masses with lesser amounts of fat, myelolipomatous degeneration of benign

Downloaded from www.ajronline.org by 45.27.234.97 on 06/22/18 from IP address 45.27.234.97. Copyright ARRS. For personal use only; all rights reserved

TABLE 1: Imaging Techniques for the Evaluation of Adrenal Nodules and Common Adrenal Lesions: Expected Imaging Findings and Other Features

Imaging Technique and Features	Lipid-Rich Adenoma	Lipid-Poor Adenoma	Pheochromocytoma	Adrenocortical Carcinoma	Myelolipoma	Metastases
CT						
Unenhanced CT	< 10 HU is diagnostic	CT histogram analysis may help characterize when nodule shows > 10% negative pixel count	Density < 10 HU due to intracytoplasmic lipid reported in only two cases	Measure ≥ 10 HU; however, areas of necrosis or cystic change can be < 10 HU	Contains large amount of bulk or macroscopic fat measuring < –10 to –20 HU	Measure ≥ 10 HU; however, areas of necrosis or cystic change can be < 10 HU
			Areas of necrosis or cystic change can be ≤ 10 HU			
Multiphase adrenal washout CT	Absolute washout > 60% and relative washout > 40% are highly specific for diagnosis	Absolute washout > 60% and relative washout > 40% are highly specific for diagnosis	≈ 30–45% can show washout in the adenoma range	Lower relative washout and absolute washout than adenomas	NA	Hypervascular metastases can washout in the adenoma range
MRI						
CSI	Visually detectable SI drop on opposed-phase imaging is specific for diagnosis	May help to characterize lipid-poor adenomas measuring between 10 and 30 HU at unenhanced CT	No case reports of pheochromocytoma showing SI drop on CSI	Limited data are available but may show SI drop on opposed-phase imaging due to intracytoplasmic lipid	Contains bulk or macroscopic fat	May show SI drop on opposed-phase imaging when the primary tumor contains fat or intracytoplasmic lipid
	SI index > 16.5% or adrenal-to-spleen SI ratio < 0.71 is specific for diagnosis	Not useful for lesions measuring ≥ 30 HU at unenhanced CT		Presence of bulk or macroscopic fat in three case reports [64–66]		
T2-weighted imaging	Usually iso- or hypointense compared with liver parenchyma or skeletal muscle		70% will be markedly hyperintense	Heterogeneously hyperintense with cystic change and necrosis possible	Follows fat SI	Usually hyperintense with cystic change and necrosis possible
	Usually homogeneous		Quantitative T2-weighted SI ratio may help differentiate from adenoma			
	When large, may show cystic degeneration					
Other features	Often incidental		Often symptomatic	Usually large (> 4 cm) at presentation with metastatic disease	May show calcifications	Personal history of malignancy
	Usually small (< 4 cm)		Biochemical testing is accurate for diagnosis; ^{123}I-MIBG has high sensitivity and high specificity for diagnosis	In the absence of metastatic disease, can be potentially differentiated from adenoma using Weiss scoring system [61, 93]		First presentation of malignancy as incidental adrenal nodule is rare
	When large, may be heterogeneous with cystic change and may undergo calcification or myelolipomatous degeneration					Can be diagnosed using FDG PET with high sensitivity and high specificity [94]

Note—NA = not applicable, CSI = chemical-shift imaging, SI = signal intensity, MIBG = metaiodobenzylguanidine.

and malignant adrenocortical tumors should be considered. ACCs are usually large heterogeneous masses that are readily differentiated from adenomas at imaging. For incidentally discovered adrenal nodules in the general population, for that are indeterminate at CECT, a 1-year follow-up is suggested to confirm stability; however, with the proliferation of DECT, a significant proportion of these adenomas can be characterized at baseline imaging potentially obviating follow-up.

References

1. Grossman A, Koren R, Tirosh A, et al. Prevalence and clinical characteristics of adrenal incidentalomas in potential kidney donors. *Endocr Res* 2016; 41:98–102
2. Young WF Jr. Clinical practice: the incidentally discovered adrenal mass. *N Engl J Med* 2007; 356:601–610
3. Blake MA, Cronin CG, Boland GW. Adrenal imaging. *AJR* 2010; 194:1450–1460
4. Lattin GE Jr, Sturgill ED, Tujo CA, et al. From the radiologic pathology archives: adrenal tumors and tumor-like conditions in the adult—radiologic-pathologic correlation. *RadioGraphics* 2014; 34:805–829
5. Berland LL, Silverman SG, Gore RM, et al. Managing incidental findings on abdominal CT: white paper of the ACR Incidental Findings Committee. *J Am Coll Radiol* 2010; 7:754–773
6. Boland GW, Blake MA, Hahn PF, Mayo-Smith WW. Incidental adrenal lesions: principles, techniques, and algorithms for imaging characterization. *Radiology* 2008; 249:756–775
7. Boland GW, Lee MJ, Gazelle GS, Halpern EF, McNicholas MM, Mueller PR. Characterization of adrenal masses using unenhanced CT: an analysis of the CT literature. *AJR* 1998; 171:201–204
8. Taner AT, Schieda N, Siegelman ES. Pitfalls in adrenal imaging. *Semin Roentgenol* 2015; 50:260–272
9. Haider MA, Ghai S, Jhaveri K, Lockwood G. Chemical shift MR imaging of hyperattenuating (>10 HU) adrenal masses: does it still have a role? *Radiology* 2004; 231:711–716
10. Boland GW. Adrenal imaging: why, when, what, and how? Part 1. Why and when to image? *AJR* 2010; 195:[web]W377–W381
11. Seo JM, Park BK, Park SY, Kim CK. Characterization of lipid-poor adrenal adenoma: chemical-shift MRI and washout CT. *AJR* 2014; 202:1043–1050
12. Caoili EM, Korobkin M, Francis IR, et al. Adrenal masses: characterization with combined unenhanced and delayed enhanced CT. *Radiology* 2002; 222:629–633
13. Peña CS, Boland GW, Hahn PF, Lee MJ, Mueller PR. Characterization of indeterminate (lipid-poor) adrenal masses: use of washout characteristics at contrast-enhanced CT. *Radiology* 2000; 217:798–802
14. Sangwaiya MJ, Boland GW, Cronin CG, Blake MA, Halpern EF, Hahn PF. Incidental adrenal lesions: accuracy of characterization with contrast-enhanced washout multidetector CT—10-minute delayed imaging protocol revisited in a large patient cohort. *Radiology* 2010; 256:504–510
15. Halefoglu AM, Bas N, Yasar A, Basak M. Differentiation of adrenal adenomas from nonadenomas using CT histogram analysis method: a prospective study. *Eur J Radiol* 2010; 73:643–651
16. Jhaveri KS, Wong F, Ghai S, Haider MA. Comparison of CT histogram analysis and chemical shift MRI in the characterization of indeterminate adrenal nodules. *AJR* 2006; 187:1303–1308
17. Remer EM, Motta-Ramirez GA, Shepardson LB, Hamrahian AH, Herts BR. CT histogram analysis in pathologically proven adrenal masses. *AJR* 2006; 187:191–196
18. Wortman JR, Bunch PM, Fulwadhva UP, Bonci GA, Sodickson AD. Dual-energy CT of incidental findings in the abdomen: can we reduce the need for follow-up imaging? *AJR* 2016 Jul 6 [Epub ahead of print]
19. Botsikas D, Triponez F, Boudabbous S, Hansen C, Becker CD, Montet X. Incidental adrenal lesions detected on enhanced abdominal dual-energy CT: can the diagnostic workup be shortened by the implementation of virtual unenhanced images? *Eur J Radiol* 2014; 83:1746–1751
20. Gnannt R, Fischer M, Goetti R, Karlo C, Leschka S, Alkadhi H. Dual-energy CT for characterization of the incidental adrenal mass: preliminary observations. *AJR* 2012; 198:138–144
21. Helck A, Hummel N, Meinel FG, Johnson T, Nikolaou K, Graser A. Can single-phase dual-energy CT reliably identify adrenal adenomas? *Eur Radiol* 2014; 24:1636–1642
22. Ho LM, Marin D, Neville AM, et al. Characterization of adrenal nodules with dual-energy CT: can virtual unenhanced attenuation values replace true unenhanced attenuation values? *AJR* 2012; 198:840–845
23. Kim YK, Park BK, Kim CK, Park SY. Adenoma characterization: adrenal protocol with dual-energy CT. *Radiology* 2013; 267:155–163
24. Connolly MJ, McGrath T, Schieda N. Diagnostic accuracy of virtual non-contrast enhanced dual-energy CT for diagnosis of adrenal adenoma: a systematic review and meta-analysis. (abstract) RSNA 2016. Oak Brook, IL: Radiological Society of North America, 2016. archive.rsna.org/2016/Monday.pdf. Accessed February 14, 2017
25. Glazer DI, Maturen KE, Kaza RK, et al. Adrenal incidentaloma triage with single-source (fast-kilovoltage switch) dual-energy CT. *AJR* 2014; 203:329–335
26. Morgan DE, Weber AC, Lockhart ME, Weber TM, Fineberg NS, Berland LL. Differentiation of high lipid content from low lipid content adrenal lesions using single-source rapid kilovolt (peak)-switching dual-energy multidetector CT. *J Comput Assist Tomogr* 2013; 37:937–943
27. Mileto A, Nelson RC, Marin D, Roy Choudhury K, Ho LM. Dual-energy multidetector CT for the characterization of incidental adrenal nodules: diagnostic performance of contrast-enhanced material density analysis. *Radiology* 2015; 274:445–454
28. Mitchell DG, Crovello M, Matteucci T, Petersen RO, Miettinen MM. Benign adrenocortical masses: diagnosis with chemical shift MR imaging. *Radiology* 1992; 185:345–351
29. Siegelman ES. Adrenal MRI: techniques and clinical applications. *J Magn Reson Imaging* 2012; 36:272–285
30. Schindera ST, Soher BJ, Delong DM, Dale BM, Merkle EM. Effect of echo time pair selection on quantitative analysis for adrenal tumor characterization with in-phase and opposed-phase MR imaging: initial experience. *Radiology* 2008; 248:140–147
31. Adam SZ, Nikolaidis P, Horowitz JM, et al. Chemical shift MR imaging of the adrenal gland: principles, pitfalls, and applications. *RadioGraphics* 2016; 36:414–432
32. Schieda N, Al Dandan O, Kielar AZ, Flood TA, McInnes MD, Siegelman ES. Pitfalls of adrenal imaging with chemical shift MRI. *Clin Radiol* 2014; 69:1186–1197
33. Ramalho M, Heredia V, de Campos RO, Dale BM, Azevedo RM, Semelka RC. In-phase and out-of-phase gradient-echo imaging in abdominal studies: intra-individual comparison of three different techniques. *Acta Radiol* 2012; 53:441–449
34. ReAm JM, Gaing B, Mussi TC, Rosenkrantz AB. Characterization of adrenal lesions at chemical-shift MRI: a direct intraindividual comparison of in- and opposed-phase imaging at 1.5 T and 3 T. *AJR* 2015; 204:536–541
35. Namimoto T, Nakamura S, Morita K, Utsunomiya D, Oda S, Yamashita Y. Fat detection of adrenal lesions using 3D 3-point Dixon MR imaging: comparison with 2D dual echo chemical shift MR imaging. (abstract) RSNA 2016. archive.rsna.org/2010/9010427.html. Oak Brook, IL: Radiological Society of North America 2010. Accessed December 2016
36. Taffel M, Haji-Momenian S, Nikolaidis P, Miller FH. Adrenal imaging: a comprehensive review. *Radiol Clin North Am* 2012; 50:219–243, v
37. Savci G, Yazici Z, Sahin N, Akgoz S, Tuncel E. Value of chemical shift subtraction MRI in characterization of adrenal masses. *AJR* 2006; 186:130–135
38. Mayo-Smith WW, Lee MJ, McNicholas MM, Hahn PF, Boland GW, Saini S. Characterization of

Downloaded from www.ajronline.org by 45.27.234.97 on 06/22/18 from IP address 45.27.234.97. Copyright ARRS. For personal use only; all rights reserved

Downloaded from www.ajronline.org by 45.27.234.97 on 06/22/18 from IP address 45.27.234.97. Copyright ARRS. For personal use only; all rights reserved

adrenal masses (< 5 cm) by use of chemical shift MR imaging: observer performance versus quantitative measures. *AJR* 1995; 165:91–95

39. Sebro R, Aslam R, Muglia VF, Wang ZJ, Westphalen AC. Low yield of chemical shift MRI for characterization of adrenal lesions with high attenuation density on unenhanced CT. *Abdom Imaging* 2015; 40:318–326
40. Gunn AJ, Seethamraju RT, Hedgire S, Elmi A, Daniels GH, Harisinghani MG. Imaging behavior of the normal adrenal on ferumoxytol-enhanced MRI: preliminary findings. *AJR* 2013; 201:117–121
41. Harman A, Chang KJ, Dupuy D, Rintels P. The long-lasting effect of ferumoxytol on abdominal magnetic resonance imaging. *J Comput Assist Tomogr* 2014; 38:571–573
42. Schieda N. Parenteral ferumoxytol interaction with magnetic resonance imaging: a case report, review of the literature and advisory warning. *Insights Imaging* 2013; 4:509–512
43. Perillo MS, Nimhuircheartaigh S, Mortele KJ. Adrenal gland iron deposition: a heretofore ignored MRI finding. (abstract) RSNA 2016. Oak Brook, IL: Radiological Society of North America, 2016. rsna2016.rsna.org/program/. Accessed February 14, 2017
44. Varghese JC, Hahn PF, Papanicolaou N, Mayo-Smith WW, Gaa JA, Lee MJ. MR differentiation of phaeochromocytoma from other adrenal lesions based on qualitative analysis of T2 relaxation times. *Clin Radiol* 1997; 52:603–606
45. Woo S, Cho JY, Kim SY, Kim SH. Adrenal adenoma and metastasis from clear cell renal cell carcinoma: can they be differentiated using standard MR techniques? *Acta Radiol* 2014; 55:1120–1128
46. Newhouse JH, Heffess CS, Wagner BJ, Imray TJ, Adair CF, Davidson AJ. Large degenerated adrenal adenomas: radiologic-pathologic correlation. *Radiology* 1999; 210:385–391
47. Miller FH, Wang Y, McCarthy RJ, et al. Utility of diffusion-weighted MRI in characterization of adrenal lesions. *AJR* 2010; 194:[web]W179–W185
48. Sandrasegaran K, Patel AA, Ramaswamy R, et al. Characterization of adrenal masses with diffusion-weighted imaging. *AJR* 2011; 197:132–138
49. Becker-Weidman D, Kalb B, Mittal PK, et al. Differentiation of lipid-poor adrenal adenomas from non-adenomas with magnetic resonance imaging: utility of dynamic, contrast enhancement and single-shot T2-weighted sequences. *Eur J Radiol* 2015; 84:2045–2051
50. Rodacki K, Ramalho M, Dale BM, et al. Combined chemical shift imaging with early dynamic serial gadolinium-enhanced MRI in the characterization of adrenal lesions. *AJR* 2014; 203:99–106
51. Song JH, Chaudhry FS, Mayo-Smith WW. The incidental adrenal mass on CT: prevalence of adrenal disease in 1,049 consecutive adrenal masses in patients with no known malignancy. *AJR* 2008; 190:1163–1168
52. Patel J, Davenport MS, Cohan RH, Caoili EM. Can established CT attenuation and washout criteria for adrenal adenoma accurately exclude pheochromocytoma? *AJR* 2013; 201:122–127
53. Park BK, Kim B, Ko K, Jeong SY, Kwon GY. Adrenal masses falsely diagnosed as adenomas on unenhanced and delayed contrast-enhanced computed tomography: pathological correlation. *Eur Radiol* 2006; 16:642–647
54. Park BK, Kim CK, Kwon GY, Kim JH. Re-evaluation of pheochromocytomas on delayed contrast-enhanced CT: washout enhancement and other imaging features. *Eur Radiol* 2007; 17:2804–2809
55. Schieda N, Alrashed A, Flood TA, Samji K, Shabana W, McInnes MD. Comparison of quantitative MRI and CT washout analysis for differentiation of adrenal pheochromocytoma from adrenal adenoma. *AJR* 2016; 206:1141–1148
56. Choyke PL, Doppman JL. Case 18: adrenocorticotropic hormone-dependent Cushing syndrome. *Radiology* 2000; 214:195–198
57. Gabriel H, Pizzitola V, McComb EN, Wiley E, Miller FH. Adrenal lesions with heterogeneous suppression on chemical shift imaging: clinical implications. *J Magn Reson Imaging* 2004; 19:308–316
58. Kenney PJ, Wagner BJ, Rao P, Heffess CS. Myelolipoma: CT and pathologic features. *Radiology* 1998; 208:87–95
59. Hindman N, Israel GM. Adrenal gland and adrenal mass calcification. *Eur Radiol* 2005; 15:1163–1167
60. Zorgdrager M, Pol R, van Hemel B, van Ginkel R. Giant adrenal myelolipoma: when trauma and oncology collide. *BMJ Case Rep* 2014; 2014:bcr2014204023
61. Lau SK, Weiss LM. The Weiss system for evaluating adrenocortical neoplasms: 25 years later. *Hum Pathol* 2009; 40:757–768
62. Montone KT, Rosen M, Siegelman ES, Fogt F, Livolsi VA. Adrenocortical neoplasms with myelolipomatous and lipomatous metaplasia: report of 3 cases. *Endocr Pract* 2009; 15:128–133
63. Wang J, Fisher C, Thway K. "Dominant" myelolipoma encasing adrenal cortical carcinoma: an unusual variation of myelolipoma occurring as a synchronous and predominant neoplasm. *Int J Surg Pathol* 2014; 22:731–735
64. Egbert N, Elsayes KM, Azar S, Caoili EM. Computed tomography of adrenocortical carcinoma containing macroscopic fat. *Cancer Imaging* 2010; 10:198–200
65. Ferrozzi F, Bova D. CT and MR demonstration of fat within an adrenal cortical carcinoma. *Abdom Imaging* 1995; 20:272–274
66. Heye S, Woestenborghs H, Van Kerkhove F, Oyen R. Adrenocortical carcinoma with fat inclusion: case report. *Abdom Imaging* 2005; 30:641–643
67. Blake MA, Kalra MK, Maher MM, et al. Pheochromocytoma: an imaging chameleon. *RadioGraphics* 2004; 24(suppl 1):S87–S99
68. Leung K, Stamm M, Raja A, Low G. Pheochromocytoma: the range of appearances on ultrasound, CT, MRI, and functional imaging. *AJR* 2013; 200:370–378
69. Guller U, Turek J, Eubanks S, Delong ER, Oertli D, Feldman JM. Detecting pheochromocytoma: defining the most sensitive test. *Ann Surg* 2006; 243:102–107
70. Motta-Ramirez GA, Remer EM, Herts BR, Gill IS, Hamrahian AH. Comparison of CT findings in symptomatic and incidentally discovered pheochromocytomas. *AJR* 2005; 185:684–688
71. Young WF Jr. Management approaches to adrenal incidentalomas: a view from Rochester, Minnesota. *Endocrinol Metab Clin North Am* 2000; 29:159–185, x
72. Ramsay JA, Asa SL, van Nostrand AW, Hassaram ST, de Harven EP. Lipid degeneration in pheochromocytomas mimicking adrenal cortical tumors. *Am J Surg Pathol* 1987; 11:480–486
73. Blake MA, Krishnamoorthy SK, Boland GW, et al. Low-density pheochromocytoma on CT: a mimicker of adrenal adenoma. *AJR* 2003; 181:1663–1668
74. Borhani AA, Hosseinzadeh K. Quantitative versus qualitative methods in evaluation of T2 signal intensity to improve accuracy in diagnosis of pheochromocytoma. *AJR* 2015; 205:302–310
75. Ilias I, Divgi C, Pacak K. Current role of metaiodobenzylguanidine in the diagnosis of pheochromocytoma and medullary thyroid cancer. *Semin Nucl Med* 2011; 41:364–368
76. Lee JE, Evans DB, Hickey RC, et al. Unknown primary cancer presenting as an adrenal mass: frequency and implications for diagnostic evaluation of adrenal incidentalomas. *Surgery* 1998; 124:1115–1122
77. Moosavi B, Shabana WM, El-Khodary M, et al. Intracellular lipid in clear cell renal cell carcinoma tumor thrombus and metastases detected by chemical shift (in and opposed phase) MRI: radiologic-pathologic correlation. *Acta Radiol* 2016; 57:241–248
78. Sydow BD, Rosen MA, Siegelman ES. Intracellular lipid within metastatic hepatocellular carcinoma of the adrenal gland: a potential diagnostic pitfall of chemical shift imaging of the adrenal gland. *AJR* 2006; 187:[web]W550–W551
79. Tariq U, Poder L, Carlson D, Courtier J, Joe BN, Coakley FV. Multimodality imaging of fat-containing adrenal metastasis from hepatocellular carcinoma. *Clin Nucl Med* 2012; 37:e157–e159
80. Schieda N, Krishna SM, McInnes MDF, et al. Utility of MRI to differentiate clear cell renal cell carcinoma (RCC) adrenal metastases from adrenal adenomas. *AJR* 2017 (in press)
81. Choi YA, Kim CK, Park BK, Kim B. Evaluation of adrenal metastases from renal cell carcinoma and

hepatocellular carcinoma: use of delayed contrast-enhanced CT. *Radiology* 2013; 266:514–520
82. Sasaguri K, Takahashi N, Takeuchi M, Carter RE, Leibovich BC, Kawashima A. Differentiation of benign from metastatic adrenal masses in patients with renal cell carcinoma on contrast-enhanced CT. *AJR* 2016; 207:1031–1038
83. Schwartz LH, Macari M, Huvos AG, Panicek DM. Collision tumors of the adrenal gland: demonstration and characterization at MR imaging. *Radiology* 1996; 201:757–760
84. Kerkhofs TM, Verhoeven RH, Van der Zwan JM, et al. Adrenocortical carcinoma: a population-based study on incidence and survival in the Netherlands since 1993. *Eur J Cancer* 2013; 49:2579–2586
85. Else T, Rodriguez-Galindo C. 5th International ACC Symposium: hereditary predisposition to childhood ACC and the associated molecular phenotype: 5th International ACC Symposium Session: not just for kids! *Horm Cancer* 2016; 7:36–39
86. Datta J, Roses RE. Surgical management of adrenocortical carcinoma: an evidence-based approach. *Surg Oncol Clin N Am* 2016; 25:153–170
87. Bharwani N, Rockall AG, Sahdev A, et al. Adrenocortical carcinoma: the range of appearances on CT and MRI. *AJR* 2011; 196:[web]W706–W714
88. Slattery JM, Blake MA, Kalra MK, et al. Adrenocortical carcinoma: contrast washout characteristics on CT. *AJR* 2006; 187:[web]W21–W24
89. Outwater EK, Blasbalg R, Siegelman ES, Vala M. Detection of lipid in abdominal tissues with opposed-phase gradient-echo images at 1.5 T: techniques and diagnostic importance. *RadioGraphics* 1998; 18:1465–1480
90. Ozsari L, Kutahyalioglu M, Elsayes KM, et al. Preexisting adrenal masses in patients with adrenocortical carcinoma: clinical and radiological factors contributing to delayed diagnosis. *Endocrine* 2016; 51:351–359
91. Fassnacht M, Arlt W, Bancos I, et al. Management of adrenal incidentalomas: European Society of Endocrinology Clinical Practice Guideline in collaboration with the European Network for the Study of Adrenal Tumors. *Eur J Endocrinol* 2016; 175:G1–G34
92. Ballian N, Adler JT, Sippel RS, Chen H. Revisiting adrenal mass size as an indication for adrenalectomy. *J Surg Res* 2009; 156:16–20
93. Weiss LM, Medeiros LJ, Vickery AL Jr. Pathologic features of prognostic significance in adrenocortical carcinoma. *Am J Surg Pathol* 1989; 13:202–206
94. Boland GW, Dwamena BA, Jagtiani Sangwaiya M, et al. Characterization of adrenal masses by using FDG PET: a systematic review and meta-analysis of diagnostic test performance. *Radiology* 2011; 259:117–126

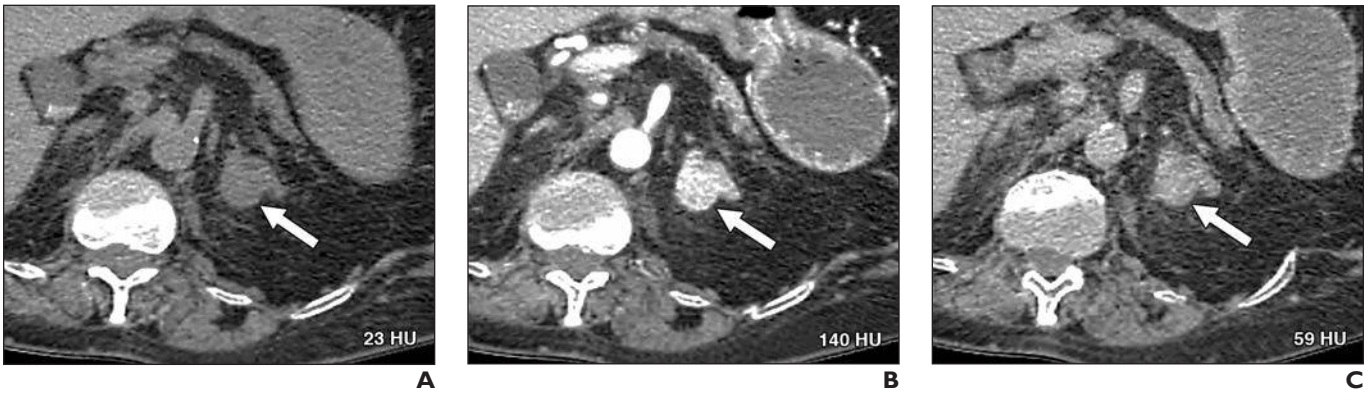

Fig. 1—72-year-old woman with history of lung cancer and indeterminate adrenal nodule detected at thoracic CT.
A, Axial unenhanced CT image shows homogeneous left adrenal nodule (*arrow*) measuring 23 HU.
B, Axial contrast-enhanced CT image obtained 70 seconds after injection of contrast material shows marked hyperenhancement of nodule (*arrow*), which measures 140 HU.
C, Axial contrast-enhanced delayed phase (15-minute) image shows washout of contrast material from nodule (*arrow*). Attenuation of nodule has decreased to 59 HU. Absolute and relative percentage washout values were 69.2% and 57.9%, respectively, which are in adenoma range. Diagnosis of adrenal adenoma was established by these findings.

Fig. 2—Examples of dual-energy CT (DECT)–derived virtual unenhanced CT data to diagnose adrenal lesions.
A, Axial 70-keV contrast-enhanced DECT image of 45-year-old woman with history of remote lung cancer shows incidentally discovered left adrenal nodule (*arrow*). Image shows homogeneous right adrenal nodule measuring 49 HU, which is indeterminate.
B, Virtual unenhanced CT image of same patient shown in **A** derived from multimaterial decomposition algorithm (Material Suppressed Iodine, GE Healthcare) shows nodule (*arrow*) has attenuation measurement of 3 HU, which is compatible with lipid-rich adenoma.
C, True unenhanced CT image of same patient obtained 2 years before **A** and **B** shows nodule (*arrow*) has not changed in size and measured –6 HU at true unenhanced CT.
(Fig. 2 continues on next page)

Downloaded from www.ajronline.org by 45.27.234.97 on 06/22/18 from IP address 45.27.234.97. Copyright ARRS. For personal use only; all rights reserved

Fig. 2 (continued)—Examples of dual-energy CT (DECT)–derived virtual unenhanced CT data to diagnose adrenal lesions.
D, 54-year-old woman with right adrenal nodule and history of colon cancer. Axial 70-keV dual-energy CECT image shows homogeneous right adrenal nodule (*arrow*) that measures 58 HU, which is indeterminate.
E, Virtual unenhanced CT image of same patient shown in **D** derived from multimaterial decomposition algorithm shows nodule (*arrow*) has attenuation measurement of 13 HU, which approaches but does not reach < 10-HU threshold to confidently diagnose adenoma.
F, True unenhanced CT image of same patient obtained 5 years before **D** and **E** shows nodule (*arrow*) has not changed in size and measured –3 HU at true unenhanced CT. In recent meta-analysis, Connolly et al. [24] reported that virtual unenhanced CT showed comparable, although slightly lower, sensitivities for diagnosis of adenoma compared with true unenhanced CT and no false-positive diagnoses.

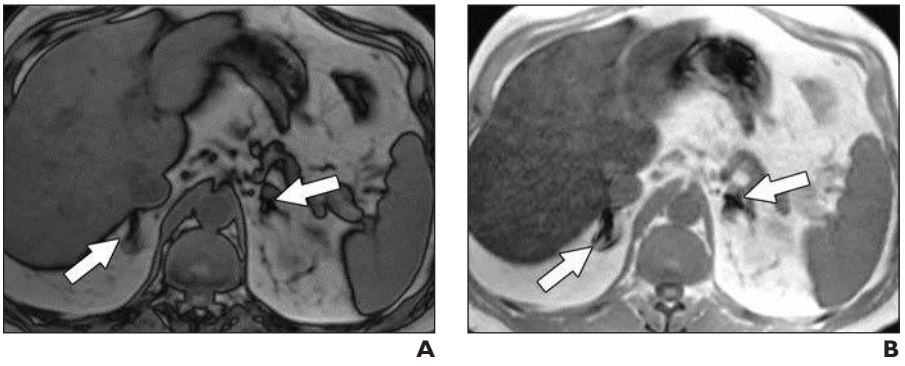

Fig. 3—68-year-old man with chronic renal insufficiency who had received IV ferumoxytol for treatment of chronic anemia.
A and **B,** Axial opposed-phase (**A**) and in-phase (**B**) T1-weighted images. Diffuse signal-intensity drop is seen on in-phase image compared with opposed-phase image because of deposition of ultrasmall iron oxide particles in adrenal glands (*arrows*). Also, note signal-intensity drop in liver and spleen on in-phase image compared with opposed-phase image.

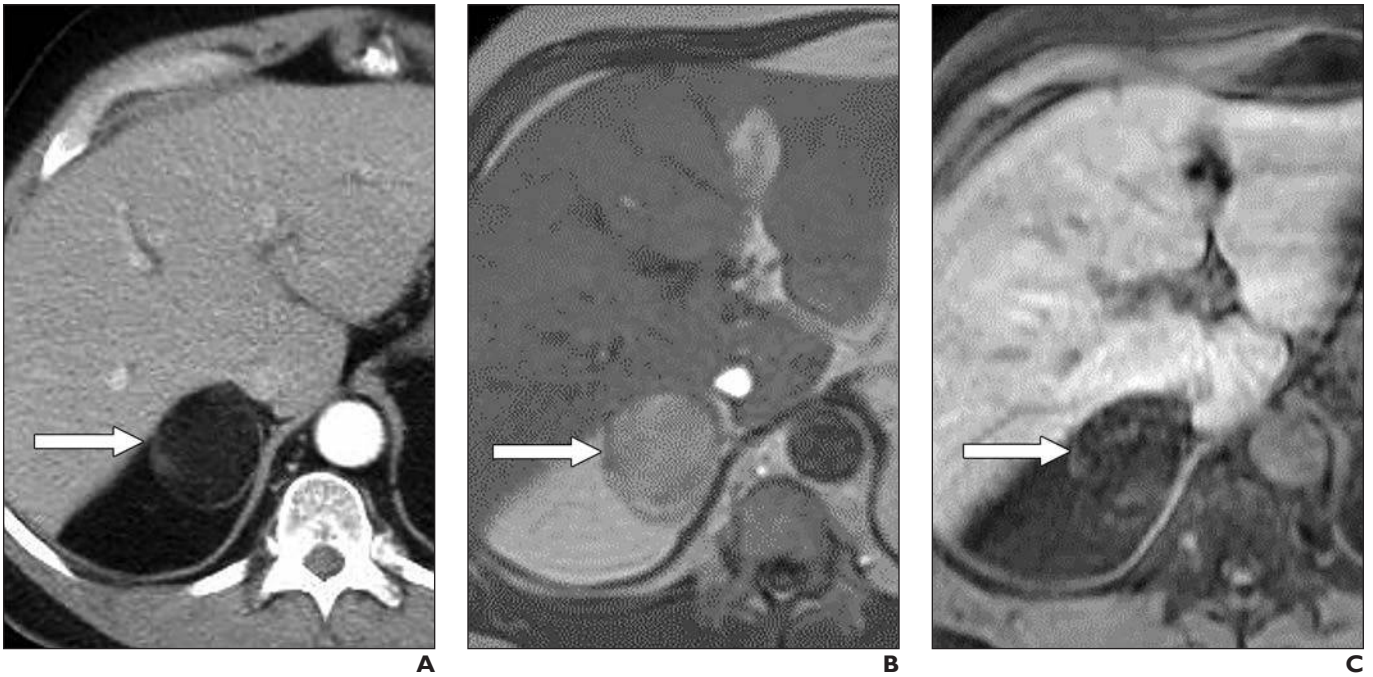

Fig. 4—Asymptomatic 58-year-old man with 5-cm right myelolipoma.
A, Axial contrast-enhanced CT image shows mainly fatty mass (*arrow*) in right adrenal gland that measures –58 HU.
B and **C,** Axial in-phase (**B**) and fat-suppressed (spectral) (**C**) T1-weighted images. Nodule (*arrow*) shows fairly homogeneous signal-intensity drop on fat-suppressed T1-weighted image.

Downloaded from www.ajronline.org by 45.27.234.97 on 06/22/18 from IP address 45.27.234.97. Copyright ARRS. For personal use only; all rights reserved

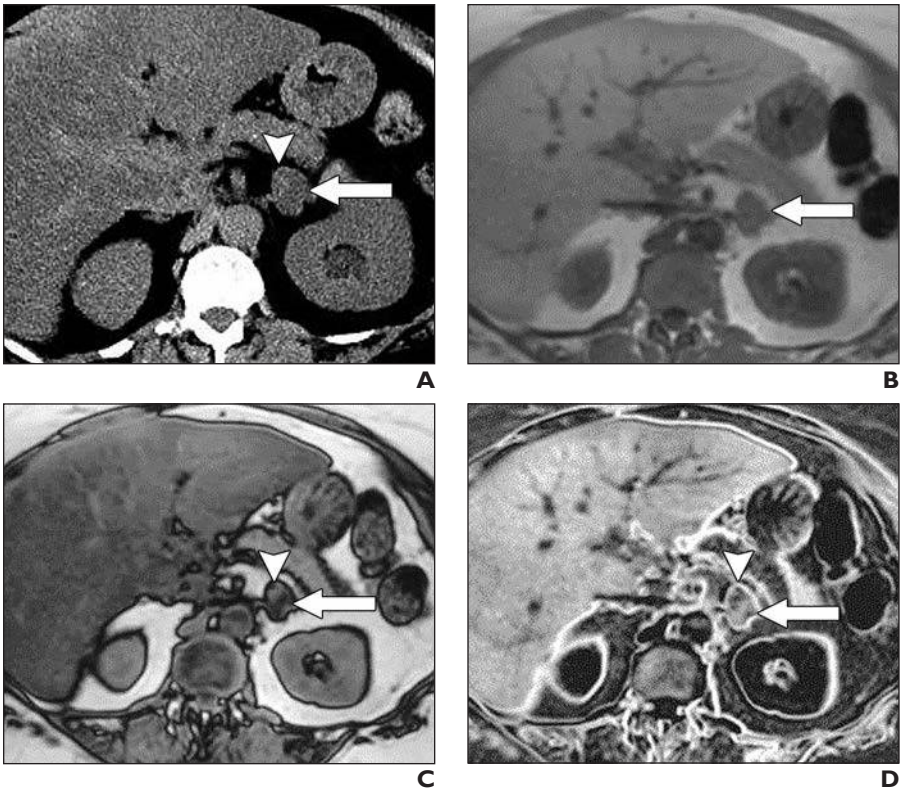

Fig. 5—61-year-old woman with incidental 2.6-cm left adrenal nodule.
A, Axial unenhanced CT image shows predominantly low-density adrenal nodule (*arrow*) with areas of increased internal attenuation (*arrowhead*). Overall mean attenuation was 20 HU.
B and **C,** Axial in-phase (**B**) and opposed-phase (**C**) T1-weighted images show heterogeneous signal-intensity drop (*arrow*). Portions of nodule do not show any signal-intensity drop (*arrowhead*, **C**) on opposed-phase image.
D, Subtraction image (in-phase minus opposed-phase) shows areas of intracellular lipid as increased signal intensity (*arrow*) and highlights portion of nodule without lipid (*arrowhead*). Nodule remained stable in size and appearance for several years and was considered heterogeneous adenoma. Also note hepatic steatosis.

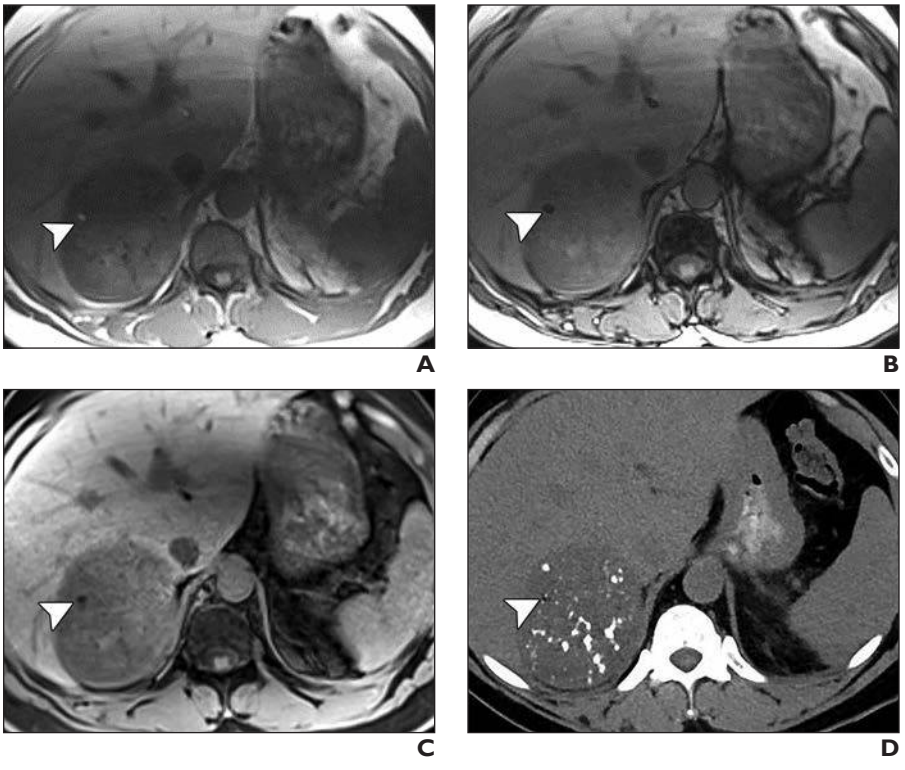

Fig. 6—55-year-old man with 11-cm right adrenal mass.
A–C, Axial in-phase (**A**), opposed-phase (**B**), and fat-suppressed (**C**) T1-weighted images show heterogeneous mass in right adrenal gland with 5-mm focus of intratumoral macroscopic fat (*arrowhead*).
D, Axial unenhanced CT image shows area of fat (*arrowhead*) with heterogeneous calcifications. Provisional diagnosis of myelolipoma was provided by interpreting radiologist. Mass was removed because of its large size, and final histopathology showed myelolipomatous degeneration of adrenocortical neoplasm.

Downloaded from www.ajronline.org by 45.27.234.97 on 06/22/18 from IP address 45.27.234.97. Copyright ARRS. For personal use only; all rights reserved

Fig. 7—56-year-old woman with right adrenal pheochromocytoma. Diagnosis was confirmed after adrenalectomy.
A, Axial unenhanced CT image shows homogeneous 3.4-cm mass (*arrow*) in right adrenal gland measuring 29 HU.
B, Axial contrast-enhanced CT image obtained 70 seconds after injection of contrast material shows marked hyperenhancement of nodule (*arrow*) that measures 131 HU.
C, Axial contrast-enhanced delayed phase (15-minute) image shows washout of contrast material from nodule (*arrow*) with attenuation that has decreased to 58 HU. Absolute and relative percentage washout values were 71.6% and 55.7%, respectively, which are in adenoma range.

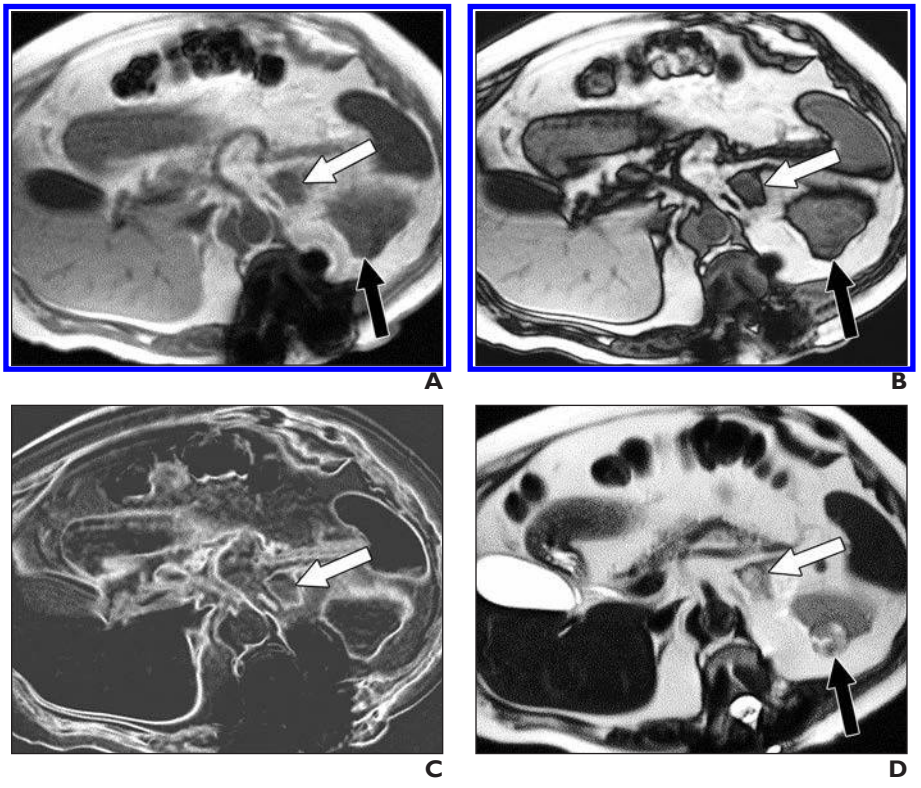

Fig. 8—67-year-old man with metastatic right clear cell renal cell carcinoma (RCC) to left adrenal gland and left kidney.
A and **B,** Axial in-phase (**A**) and opposed-phase (**B**) T1-weighted images show left adrenal metastasis (*white arrow*) and left renal metastasis (*black arrow*). There is signal-intensity drop within adrenal nodule on opposed-phase image compared with in-phase image but not within renal mass.
C, Subtraction image (in-phase minus opposed-phase) confirms presence of intracellular lipid (*arrow*), which is of increased signal intensity on subtraction imaging, in adrenal metastasis.
D, Axial T2-weighted single-shot turbo spin-echo image shows that both adrenal metastasis (*white arrow*) and renal metastasis (*black arrow*) are heterogeneous and of markedly increased signal intensity compared with skeletal muscle. Presence of intracellular lipid in clear cell RCC adrenal metastases is widely reported; however, heterogeneity and increased signal intensity on T2-weighted images are newly described features that may enable differentiation from benign adenomas [80]. Alternative strategy would be to perform biopsy or short-term (< 6 months) imaging follow-up to document growth. Previously, Moosavi et al. [77] described that not all metastases will show intracellular lipid in clear cell RCC and that, in some instances, primary tumor may also show no lipid at MRI despite presence of lipid within documented metastases in same patient. Note also spinal hardware in this patient related to previous fusion of thoracolumbar spine.

Downloaded from www.ajronline.org by 45.27.234.97 on 06/22/18 from IP address 45.27.234.97. Copyright ARRS. For personal use only; all rights reserved

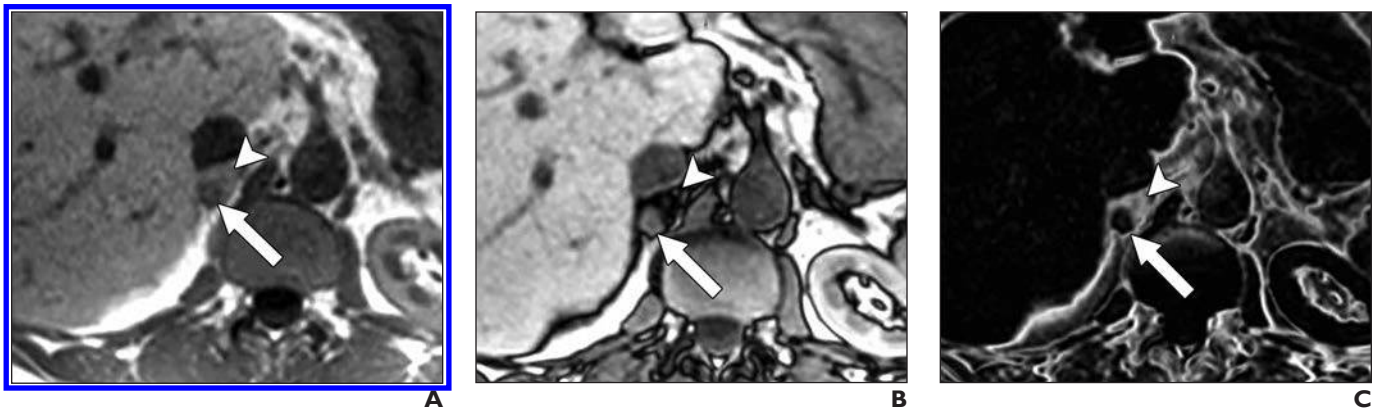

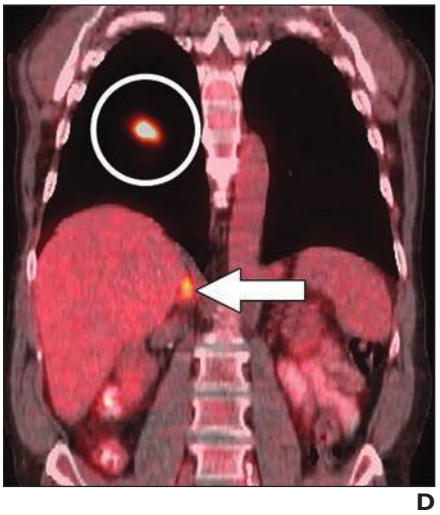

Fig. 9—67-year-old man with lung cancer and adrenal collision tumor (metastasis and adenoma).
A–C, Axial in-phase (**A**), opposed-phase (**B**), and subtraction (i.e., in-phase minus opposed-phase) (**C**) T1-weighted images show heterogeneous right adrenal lesion measuring 20 mm. Portions of lesion show signal-intensity drop (*arrowhead*) when comparing opposed-phase image with in-phase image. These portions of lesion are of increased signal intensity on subtraction image, which is indicative of intracellular lipid. Rounded 8-mm posterior portion of lesion (*arrow*) does not show signal-intensity drop. In context of known malignancy in this patient, possibility of adrenal collision tumor was raised.
D, Coronal fused FDG PET/CT image shows markedly increased FDG activity (*arrow*) within lesion; this finding confirms diagnosis of metastasis. Also note right lung cancer (*circle*).

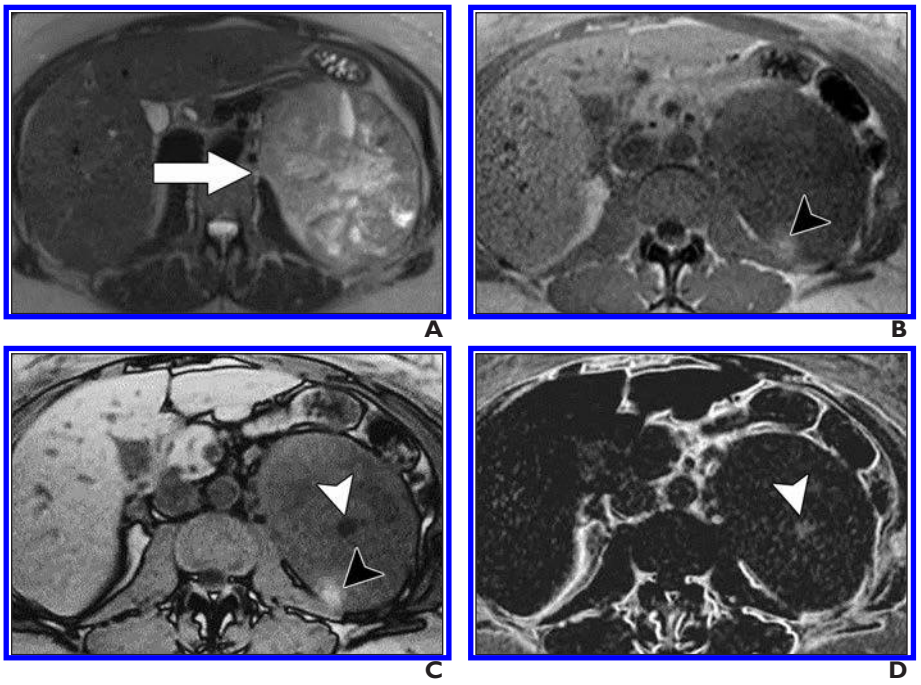

Fig. 10—50-year-old woman with adrenocortical carcinoma.
A, Axial T2-weighted single-shot turbo spin-echo image shows heterogeneous 15-cm left adrenal mass (*arrow*) is exhibiting increased signal intensity.
B–D, Axial in-phase (**B**), opposed-phase (**C**), and subtraction (i.e., in-phase minus opposed-phase) (**D**) T1-weighted images show areas of internal hemorrhage (*black arrowheads*, **B** and **C**) and intracellular lipid (*white arrowheads*, **C** and **D**).

Downloaded from www.ajronline.org by 45.27.234.97 on 06/22/18 from IP address 45.27.234.97. Copyright ARRS. For personal use only; all rights reserved

This article has been cited by:

1. Bernhard Krauss. 2018. Dual-Energy Computed Tomography. *Radiologic Clinics of North America* **56**:4, 497-506. [Crossref]
2. Desiree E. Morgan. 2018. The Role of Dual-Energy Computed Tomography in Assessment of Abdominal Oncology and Beyond. *Radiologic Clinics of North America* **56**:4, 565-585. [Crossref]
3. Benjamin Wilson, Allison Becker, Thomas Estes, Jayanth Keshavamurthy, Darko Pucar. 2018. Adrenal Hemangioma Definite Diagnosis on CT, MRI, and FDG PET in a Patient With Primary Lung Cancer. *Clinical Nuclear Medicine* **43**:6, e192-e194. [Crossref]
4. Simon S. Martin, Sebastian Weidinger, Rouben Czwikla, Benjamin Kaltenbach, Moritz H. Albrecht, Lukas Lenga, Thomas J. Vogl, Julian L. Wichmann. 2018. Iodine and Fat Quantification for Differentiation of Adrenal Gland Adenomas From Metastases Using Third-Generation Dual-Source Dual-Energy Computed Tomography. *Investigative Radiology* **53**:3, 173-178. [Crossref]
5. Joseph M. Pappachan, Nyo Nyo Tun, Ganesan Arunagirinathan, Ravinder Sodi, Fahmy W. F. Hanna. 2018. Pheochromocytomas and Hypertension. *Current Hypertension Reports* **20**:1. . [Crossref]
6. Mary M. Salvatore, Ronaldo Collo Go, Monica A. Pernia M.. The Upper Abdomen 131-145. [Crossref]

Downloaded from www.ajronline.org by 45.27.234.97 on 06/22/18 from IP address 45.27.234.97. Copyright ARRS. For personal use only; all rights reserved